

The El Niño–Southern Oscillation (ENSO) Modoki signal in the stratosphere

I. Zubiaurre¹ and N. Calvo^{1,2}

Received 9 August 2011; revised 20 December 2011; accepted 20 December 2011; published 23 February 2012.

[1] El Niño–Southern Oscillation (ENSO) is known to be the largest source of interannual variability in the tropical troposphere. However, the variability in the tropical Pacific since 1979 seems to be associated not only with “canonical” ENSO events but also with a variation thereof known as ENSO Modoki, which is characterized by warm anomalies in the central Pacific, west from those occurring during a typical ENSO. This work analyzes the signal of ENSO Modoki in the stratosphere and compares it to canonical ENSO by using the chemistry-climate Whole Atmosphere Community Climate Model (WACCM3.5). The results reveal a significant warming in the Southern Hemisphere polar stratosphere during boreal winter months, which propagates downward in early spring; this is absent during canonical warm ENSO events. On the other hand, in the Northern Hemisphere stratosphere, the anomalous warming typical of canonical El Niño episodes during boreal winter is not statistically significant during El Niño Modoki events. These differences are related in WACCM3.5 to changes in tropical convection and tropospheric teleconnections associated with each type of event. In particular, an enhancement and westward displacement of the anomalous convective area during El Niño Modoki episodes is related to an intensification of the Pacific South American teleconnection pattern and a weakening of the Aleutian Low. During cold ENSO Modoki events a significant anomalous cooling is present in the model simulations.

Citation: Zubiaurre, I., and N. Calvo (2012), The El Niño–Southern Oscillation (ENSO) Modoki signal in the stratosphere, *J. Geophys. Res.*, 117, D04104, doi:10.1029/2011JD016690.

1. Introduction

[2] El Niño–Southern Oscillation (ENSO) refers to two phenomena that take place in the tropics. El Niño is characterized by an anomalous warming of the tropical eastern Pacific Ocean that leads to heavy rainfall in this area. The Southern Oscillation is a large-scale variation of the atmospheric pressure system in the tropics, which alters trade winds and precipitation. The physical mechanism that controls ENSO has its origin in atmosphere–ocean coupling.

[3] In the tropical troposphere, ENSO is the most important source of interannual variability. In the stratosphere, the quasi-biennial oscillation (QBO) and volcanic aerosols seem to be the most influential factors of tropical variability [Calvo *et al.*, 2004]. Despite being neither a stratospheric phenomenon nor one of the main sources of variability in the stratosphere, ENSO has a significant impact in both the tropical and extratropical stratosphere. The ENSO signal propagates into the stratosphere via ultralong Rossby waves in Northern Hemisphere (NH) winter. During the warm ENSO phase, vertical wave propagation and dissipation

intensifies in the NH high latitudes during boreal winter months. Thus, the mean flow decelerates and the stratospheric mean meridional circulation becomes stronger. As a result, an anomalous cooling appears in the tropical stratosphere and an anomalous warming develops in the Arctic stratosphere [e.g., García-Herrera *et al.*, 2006]. Recent studies have also shown that the stratosphere behaves as an intermediary between the ENSO signal in the tropical troposphere and tropospheric teleconnections in the NH [Bell *et al.*, 2009; Cagnazzo and Manzini, 2009] becoming a source of winter European predictability [Ineson and Scaife, 2009].

[4] In the last decades, tropical Pacific variability has been related to two different types of ENSO episodes [Kao and Yu, 2009]. The frequency, amplitude and localization of the well-known ENSO anomaly patterns are changing, and this has motivated a re-examination of the evolution of ENSO events in the Tropical Pacific. In 2003, the NOAA defined El Niño as a phenomenon that takes place in the equatorial Pacific Ocean and it is characterized by a sea surface temperature (SST) increase of 0.5 K over the region of the tropical Pacific Ocean known as El Niño 3.4 (N3.4). However, the anomalous warming during the 2004 event extended toward El Niño 4 (N4) region (westward of the N3.4 region and close to the dateline), while temperatures in the eastern and western Pacific were cooler than normal. Ashok *et al.* [2007] named this event as “El Niño Modoki,” a

¹Departamento Física de la Tierra, Astrofísica y Astronomía, Universidad Complutense de Madrid, Madrid, Spain.

²Atmospheric Chemistry Division, Advanced Study Program, National Center for Atmospheric Research, Boulder, Colorado, USA.

term taken from the Japanese language (*Modoki* means “similar but different”). Several studies have pointed to anthropogenic and natural climate variability as possible reasons for the increase in El Niño Modoki frequency observed since 1979 [Yeh *et al.*, 2009; Ashok *et al.*, 2007]. Pseudo-Niño, dateline El Niño, central Pacific El Niño (CP El Niño) or warm pool El Niño (WP El Niño) are other terms used to denote this new phenomenon [Ashok *et al.*, 2007; Yeh *et al.*, 2009; Kao and Yu, 2009; Kug *et al.*, 2009], while the more traditional El Niño has also been referred to as canonical El Niño, eastern Pacific El Niño, or cold tongue El Niño. In this study, the terms ENSO Modoki and Canonical ENSO will be used to refer to the two types of ENSO events, while El Niño Modoki and canonical El Niño will be used to denote their warm phases.

[5] As mentioned earlier, sea surface temperature anomalies (SSTA) are key to distinguish both phenomena. Most of the ENSO Modoki anomalies (SST and winds), appear in the central Pacific. The phenomenon is governed by an advective feedback (i.e., zonal advection of mean SST by anomalous zonal currents) [Kug *et al.*, 2009] and tends to originate, develop and disappear in the tropical central Pacific in situ [Kao and Yu, 2009], not necessarily followed by the opposite phase. This difference in SSTA with respect to canonical El Niño also affects the Walker cell: during an El Niño Modoki event, two cells with ascent in the tropical central Pacific and descent in the eastern and western Pacific give rise to precipitation around the dateline [Ashok *et al.*, 2007; Weng *et al.*, 2007, 2009].

[6] Differences in teleconnection have also been found between the two phenomena [Weng *et al.*, 2007, 2009; Kao and Yu, 2009; Kim *et al.*, 2009]. During El Niño Modoki, the teleconnections in the southern part of the Indian Ocean are larger, intensifying the monsoons, one of the largest sources of tropical-extratropical teleconnections. The Pacific North American (PNA) teleconnection pattern and even teleconnections in the Atlantic Ocean are also different from those during canonical El Niño events. In addition, the frequency and settlement of the cyclogenesis in tropical and middle latitudes also differ between the two types of ENSO [Kim *et al.*, 2009].

[7] In the stratosphere, Hurwitz *et al.* [2011b] recently studied the response to these new events (characterized by the N4 index) over the Antarctic region using several reanalysis data sets (National Centers for Environmental Prediction, NCEP; ERA-40; and Modern-Era Retrospective Analysis for Research and Applications, MERRA). They found a significant warming in the lower Southern Hemisphere (SH) polar stratosphere related to a southward displacement of the South Pacific Convergence Zone (SPCZ) only when N4 events coincided with the east phase of the QBO. However, because of the small number of events that occurred during the satellite era, only a few cases were considered in each composite, which limited the generalization of their conclusions. In a follow-up study, Hurwitz *et al.* [2011a] analyzed the WP El Niño signal in simulations of the Goddard Earth Observing System chemistry-climate model version 2 (GEOS V2 CCM) without volcanic and solar variability. These were time-sliced simulations with composited SST as boundary conditions from a certain number of observed warm pool ENSO and neutral ENSO

events. GEOS V2 CCM was able to simulate the signal found in the Antarctic stratosphere in reanalysis data, although weaker in amplitude. In addition, in contrast to the results of the study by Hurwitz *et al.* [2011b], this response was not sensitive to the phase of the internally modeled generated QBO, probably related to the unrealistic QBO signal in the tropical lower stratosphere and upper troposphere, as the authors pointed out.

[8] In our study, we will make use of four transient ensemble simulations of the Whole Atmosphere Community Climate Model (WACCM3.5), run with observed SST and a nudged QBO following observations, to investigate the stratospheric signal of El Niño Modoki in comparison with canonical El Niño events. Their propagation mechanisms will be analyzed in both cases to understand the differences. This characterization will be essential to predict the possible ENSO Modoki influence on the stratospheric circulation, tracer constituents, and perhaps, eventually, the troposphere. The cold phase of ENSO Modoki (La Niña Modoki), characterized by an anomalous cooling in the central Pacific and flanked by anomalous warming in the eastern and western Pacific [Ashok and Yamagata, 2009], will also be investigated.

[9] This article is organized as follows: section 2 presents the data and methodology; the signals of El Niño Modoki and canonical El Niño in the stratosphere are described in section 3 while section 4 investigates the tropospheric forcings. Sections 5 and 6 discuss the main results and present the main conclusions, respectively.

2. Data and Method

2.1. Model Data

[10] WACCM3.5 is a fully interactive chemistry-climate model (CCM) that spans from the surface to approximately 140 km. It is based on version 3 of the Community Atmospheric Model (CAM) and incorporates most of the physical and chemical processes required to model the middle atmosphere, including the mesosphere and lower thermosphere. This version of the model is the same as the one used by Calvo *et al.* [2010]. A short description of the model can be found in their study.

[11] The present study employs a four-member ensemble of simulations run at horizontal resolution of 1.9° latitude by 2.5° longitude from 1953 to 2004. The model produces a QBO by relaxing the tropical winds to observations [Matthes *et al.*, 2004] and calculates heating from volcanic aerosols [Tilmes *et al.*, 2009]. SST and loadings of greenhouse gases and halogen species are prescribed from observations, as explained by García *et al.* [2007]. The simulations are part of the second CCM validation activity (CCMVal2) of the Stratospheric Processes and Their Role in Climate (SPARC) project [Stratospheric Processes and Their Role in Climate Chemistry-Climate Models Validation Group, 2010].

[12] In order to isolate the ENSO signal from other sources of variability, which are important in the stratosphere, a multilinear regression has been performed, following the methodology explained by Calvo *et al.* [2010]. The monthly mean ensemble mean series was deseasonalized and then regressed onto different predictors, which accounted for the long-term trend, the 11 year solar cycle, the QBO, and the

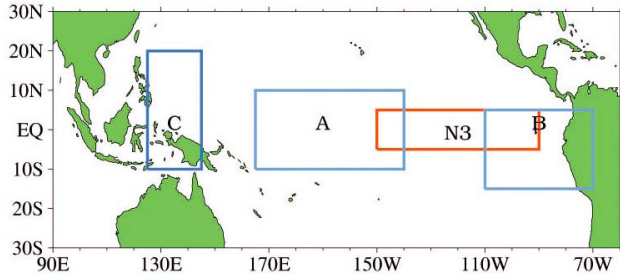


Figure 1. Representation of the regions (A, B, and C boxes) employed to calculate the EMI index and N3 index.

effects of volcanic eruptions. A linear trend was used to estimate long-term trends, the solar f10.7 radio flux was used as a predictor for the 11 year solar cycle, and the QBO variability was extracted using two orthogonal time series, as in the study by *Randel and Wu* [1996]. Volcanic effects were represented in terms of an aerosol optical depth (AOD) index, as in the study by *Calvo et al.* [2004]; as no major volcanic eruptions have occurred from 2000 to the end of the simulations, no update of the AOD index was necessary. The ENSO signal is then included in the residual of the multiple linear regression, which was also smoothed to eliminate subseasonal fluctuations by taking a three-point boxcar average. This final product is the series used in the analysis of the two different ENSO phenomena. Recent studies have shown that the ENSO signal in the extratropics might interact nonlinearly with other sources of variability such as the QBO or the 11 year solar cycle [*Garfinkel and Hartmann*, 2007; *Calvo et al.*, 2009; *Calvo and Marsh*, 2011]; these nonlinear interactions are not taken into account in a multivariate linear regression. However, as discussed in the following, the comparison of our results with those from a previous version of the model (WACCM1b), where no QBO was simulated and no 11 year solar cycle variability is considered, shows a good agreement overall, which adds confidence to the methodology employed here. If the composites were calculated without performing a multiple linear regression, the main differences in the temperature response to El Niño Modoki are twofold. First, the significance of El Niño Modoki signal in the SH over the polar cap is reduced because of the larger polar variability included in the data series. Second, the warming in the tropical troposphere is larger, probably related to the long-term trend associated with the increase in greenhouse gases.

[13] As boundary conditions, WACCM3.5 prescribes SST data from the Hadley Centre (HadISST) of the U.K. Met Office [*Rayner et al.*, 2003]. This data set has also been used to compute the ENSO indices as will be explained in the following. HadISST consists of monthly mean fields of SST and sea-ice concentration from 1870. Missing values are filled in a statistically optimal way. HadISST therefore has global coverage and is available on a 1° latitude \times 1° longitude grid.

2.2. ENSO Modoki and ENSO Indices

[14] To characterize ENSO Modoki events, and because of the unique tripolar nature of the SSTA (positive anomalies in the central Pacific and negative anomalies in the

eastern and western Pacific), *Ashok et al.* [2007] defined El Niño Modoki Index (EMI) as follows:

$$\text{EMI} = [\text{SSTA}]_A - 0.5[\text{SSTA}]_B - 0.5[\text{SSTA}]_C \quad (1)$$

The square bracket in equation (1) represents the area-averaged SSTA over each of the regions A (165°E – 140°W , 10°S – 10°N), B (110°W – 70°W , 15°S – 5°N), and C (125°E – 145°E , 10°S – 20°N), respectively, displayed in blue boxes in Figure 1.

[15] *Ashok et al.* [2007] analyzed the SST variability over the tropical Pacific Ocean using Empirical Orthogonal Functions (EOF). They showed that the first two modes represented most of the Pacific variability over the 1979–2004 period. The first mode was associated with canonical El Niño and the second one with El Niño Modoki. A correlation analysis showed that the correlation coefficient between the second principal component (PC2) and EMI was 0.91, which gives consistency to the definition of this index. When the analyzed period was extended backward in time, the second mode of variability did not show a maximum in variance in the central Pacific, characteristic of Modoki events. In particular, EOF2 for 1958–1970 was also associated with the canonical El Niño pattern. This is why the ENSO Modoki signal is analyzed here only during the 1979–2004 period.

[16] Canonical ENSO events are characterized by El Niño 3 (N3) index. This index is defined as the SSTA averaged over the N3 region (150°W – 90°W , 5°S – 5°N) (red box in Figure 1). According to *Ashok et al.* [2007], the correlation between their PC1 and N3 index is very high, 0.98. The N3.4 index (region 120°W – 170°W , 5°N – 5°S) has not been used in our analysis because it includes SSTA that belong to the equatorial central Pacific region used to characterize Modoki events [*Weng et al.*, 2007].

[17] The temporal evolution of EMI and N3 index, after normalization and subtraction of the subseasonal fluctuation with a three-point boxcar average, is shown in Figure 2.

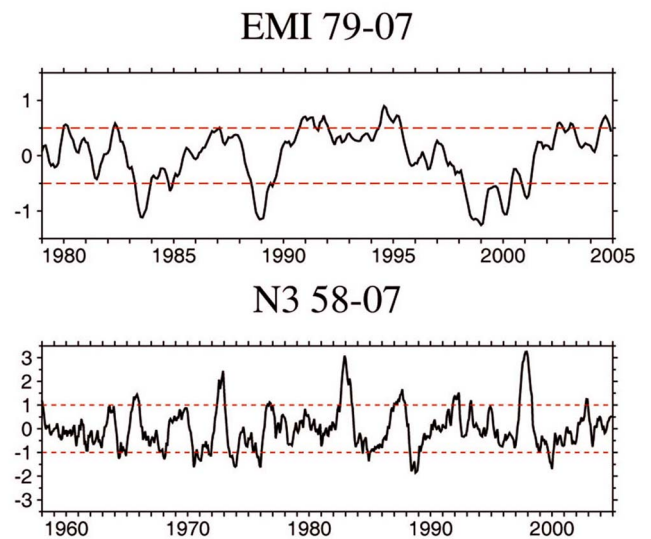


Figure 2. (top) Temporal evolution of the EMI index from 1979 to 2006 and (bottom) temporal evolution of the N3 index from 1958 to 2006.

Table 1. Maximum Values of EMI for El Niño Modoki Events, N3 for Extreme Canonical El Niño Events, and EMI for La Niña Events^a

El Niño Modoki		Extreme Niño 3		La Niña Modoki	
Event	EMI	Event	N3	Event	EMI
February 1980	0.5628	December 1972	2.4388	August 1983	−1.1230
February 1987	0.5052	December 1982	3.0789	November 1984	−0.6638
January 1991	0.7042	December 1997	3.2506	December 1988	−1.1760
November 1991	0.7269			January 1999	−1.2618
August 1994	0.8958			February 2000	−1.0626
February 2003	0.5837			February 2001	−0.7669

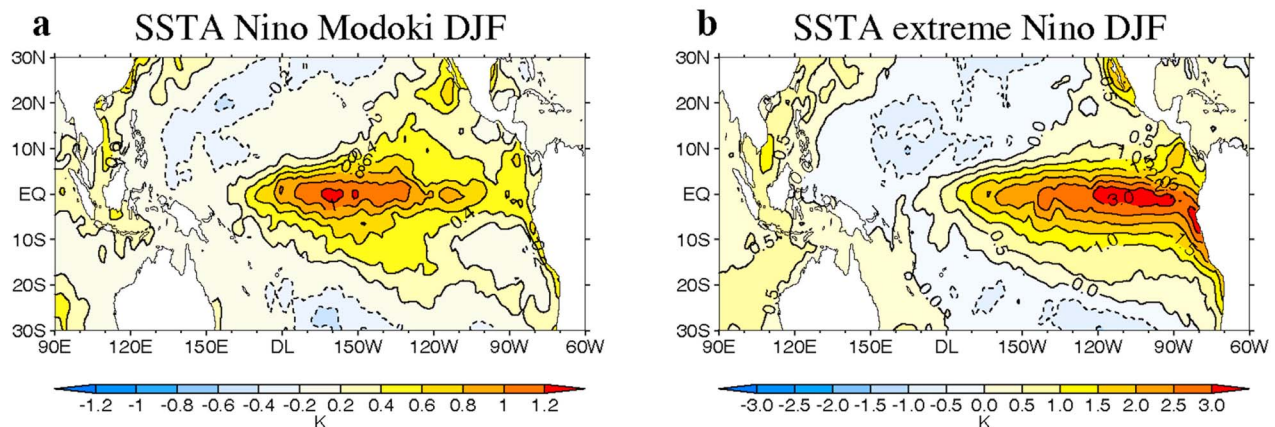
^aEMI, El Niño Modoki Index; N3, El Niño 3 Index.

El Niño and La Niña Modoki events are identified whenever EMI exceeds ± 0.5 standard deviations. Table 1 lists the warm and cold ENSO Modoki episodes selected and their corresponding EMI values. The warm event that peaked in October 1982 was not considered as an El Niño Modoki event in our study because its SSTA show a strong canonical El Niño pattern. The events listed in Table 1 coincide with those chosen by other authors who studied the phenomenon in the troposphere [Ashok *et al.*, 2007; Weng *et al.*, 2007, 2009]. In our study, only the most extreme canonical El Niño events have been chosen following the study by Kug *et al.* [2009]. These events show strong positive SSTA in the eastern Pacific that are essentially different from those of El Niño Modoki. Table 1 and Figure 2 show clearly that N3 values are much larger than those from EMI. In addition, Modoki events seem to peak more broadly around the boreal winter months than the canonical El Niño events. However, all the El Niño Modoki events selected have EMI values exceeding 0.5 standard deviations during boreal winter months.

[18] Composites for El Niño Modoki and canonical El Niño events listed in Table 1 have been computed from boreal summer to boreal spring. Most of the plots shown here, display boreal winter months, as they capture most of the signal and facilitate the comparison with canonical ENSO episodes, whose stratospheric signal is known to maximize at the same time. Figure 3a shows the SSTA

composite for El Niño Modoki events for the December-January-February average. As expected, the anomalies display the tripolar structure characteristic of El Niño Modoki events and justify the regions selected in the EMI definition: positive SSTA up to 1.2 K in the central Pacific and negative anomalies up to 0.4 K to the east and west of the positive anomaly. Both the magnitudes and the extension of the anomalies resemble those shown by Ashok *et al.* [2007], which gives consistency to our choice of El Niño Modoki episodes. Although the positive SSTA for the extreme canonical El Niño episodes are almost three times larger than the ones for El Niño Modoki (Figure 3), the negative SSTA values are approximately the same for the two phenomena.

[19] The significance of the composite anomalies with respect to the internal variability of the model has been tested by a Monte Carlo method. First, for each calendar month, a random group of the same number of cases ($n = 6$, see Table 1) as El Niño Modoki events used in the composites we want to test has been chosen. The random group is created from the entire 1953–2004 time series. Then, the composite of this group has been computed. This procedure has been repeated 1000 times and the distribution plotted. A preliminary analysis showed that 1000 realizations were enough to estimate the probability distribution properly. The sample follows a normal distribution, so that the 2.5% tails lay at approximately ± 1.96 standard deviations from the

**Figure 3.** Composites of sea surface temperature anomalies (SSTA) for (a) El Niño Modoki events (contours drawn every 0.2 K) and (b) canonical El Niño extreme events during the December-January-February (DJF) period (contours drawn every 0.5 K).

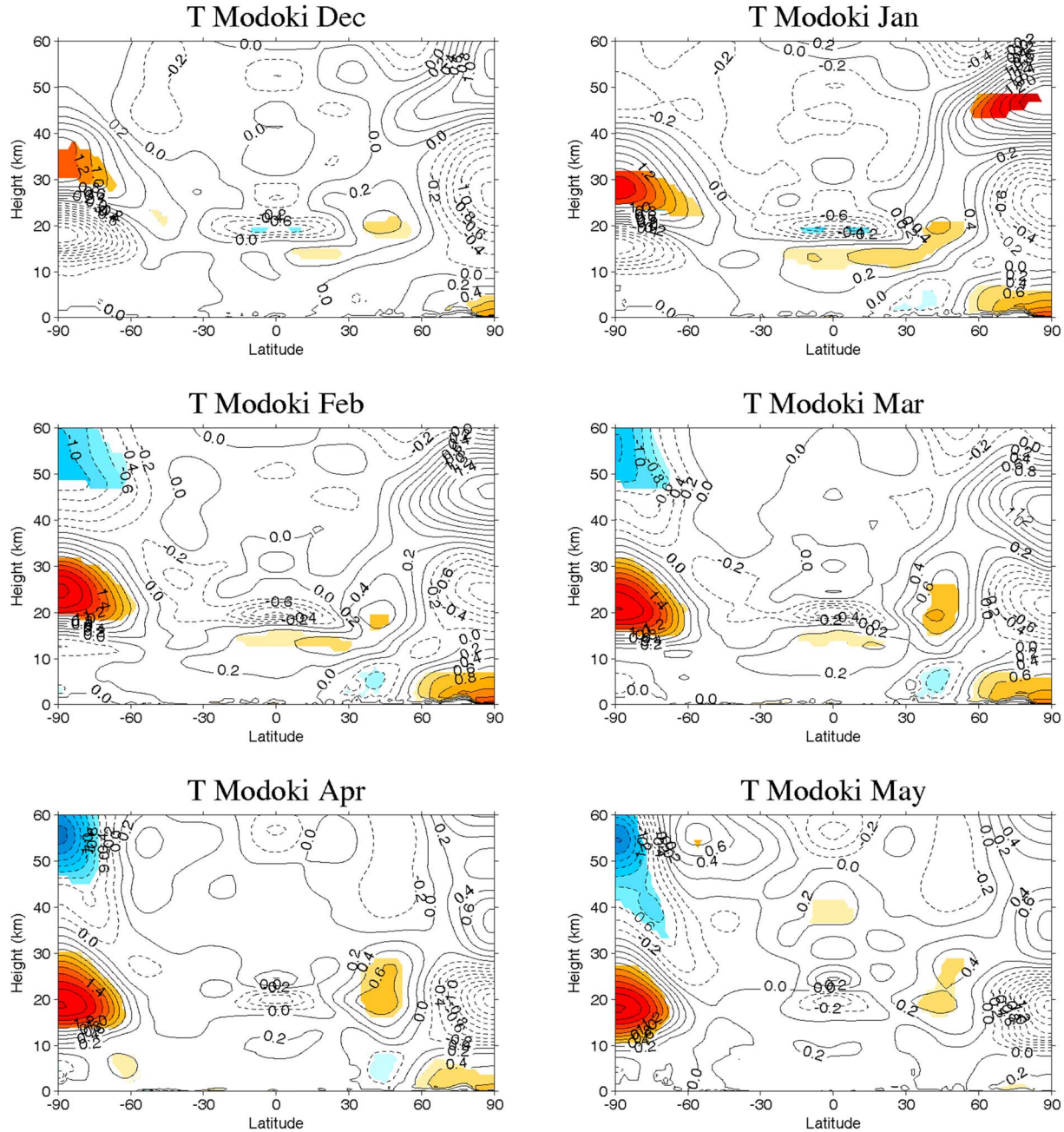


Figure 4. Cross section (height vs. latitude) of the composites of zonal mean temperature anomalies for El Niño Modoki events from December to May as explained in the text. Colored regions are significant at the 95% level according to a Monte Carlo test. Contours are drawn every 0.2 K.

mean. These are the thresholds above or below which the composite anomalies are considered to be 95% significant.

3. El Niño Modoki Signal in the Stratosphere

[20] Composites of zonal mean temperature anomalies for El Niño Modoki events are shown in Figure 4 from December to May. The largest signal is found in the SH polar region, where an anomalous significant warming is observed first in December at around 35 km and lasts until

September (not shown). Polar temperature anomalies reach their maximum (about 2 K) in February and retain this large amplitude until July (not shown). An anomalous significant cooling appears in February in the polar mesosphere, above the significant warming, and intensifies (up to -1.5 K) as boreal spring begins. In the NH, a dipole with anomalous warming in the upper stratosphere-lower mesosphere (35–60 km) and anomalous cooling in the lower stratosphere (15–30 km) is present, but it is not significant. In the tropics, a weak but significant anomalous

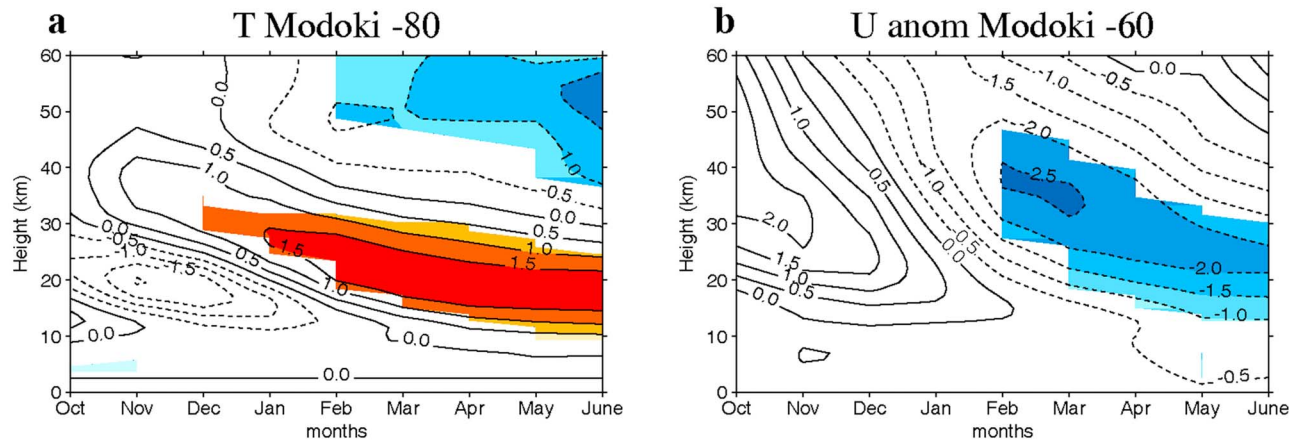


Figure 5. October–June composites of zonal mean temperature anomalies at (a) 80°S (contours drawn every 0.5 K) and (b) zonal mean zonal wind anomalies at 60°S for El Niño Modoki events (contours drawn every 0.5 m s⁻¹). Colored regions are significant at the 95% level according to a Monte Carlo test.

warming occurs in the upper troposphere from January to March. In the lowermost tropical stratosphere, negative anomalies (of up to -0.6 K) appear from December to April, although they are significant only during the first two months.

[21] From the preceding description, it is clear that the largest impact of El Niño Modoki in zonal mean temperature occurs as a significant warming in the SH polar region. This is in agreement with the study by *Hurwitz et al.* [2011b] who found a significantly warmer SH lower polar stratosphere in ERA-40 data for the November–December average during strong warm N4 events. The temporal evolution of the signal shown in the different plots in Figure 4 also indicates that the dipole structure formed by anomalous significant warming below and cooling above propagates downward from the upper stratosphere–lower mesosphere to the lower stratosphere. This is illustrated in Figure 5a, which represents the time–height cross section of zonal mean temperature anomalies for El Niño Modoki composites at 80°S. This diagnostic was first used by *Manzini et al.* [2006] to illustrate the downward propagation of the stratospheric ENSO signal in the NH. Figure 5 shows positive significant temperature anomalies moving downward and intensifying, from the middle stratosphere in December to the lower stratosphere in May, together with negative significant anomalies propagating downward from the lower mesosphere to the upper stratosphere. The signal in temperature is accompanied by anomalies in zonal mean zonal wind (Figure 5b), as expected from the geostrophic balance. Significant negative anomalies in zonal mean zonal winds appear in February in the upper stratosphere and continue until June, when they reach the lower stratosphere and even the troposphere.

[22] The signal of El Niño Modoki in zonal mean temperature is compared with that from canonical El Niño events. Composites of zonal mean temperature for the N3 extreme events are displayed in Figure 6. In this case, the significance should be treated cautiously, as only three episodes are considered, as explained in section 2. During canonical El Niño episodes, most of the significant signal appears in the NH as a temperature dipole formed by

anomalous warming in the stratosphere and anomalous cooling in the mesosphere. These anomalies propagate downward reaching the tropopause in February. Significant anomalous warming in the stratosphere is present from December to March, the largest being in February (up to 6.5 K). In contrast, very small regions of statistically significant signal are found during canonical El Niño events in the SH. In the tropics, an anomalous warming of about 0.5–1 K is simulated in the troposphere. It reaches a maximum in February, both in magnitude and spatial extension. Above it, an anomalous cooling is observed in the lower stratosphere, which reaches up to 2 K in February and weakens thereafter. Despite having composited only three events, which are essentially different from El Niño Modoki episodes, the signal obtained in both tropics and extratropics is consistent with that reported in the literature from models and observations [*Sassi et al.*, 2004; *García-Herrera et al.*, 2006; *Manzini et al.*, 2006; *Free and Seidel*, 2009; *Calvo et al.*, 2010], and therefore, useful for our comparison with El Niño Modoki.

[23] The comparison of Figures 4 and 6 highlights the main differences in zonal mean stratospheric signals between the two types of El Niño events. First, the tropical signal observed during El Niño Modoki events is weaker than during the canonical ENSO episodes. This is not surprising as weaker SSTa are typical of El Niño Modoki events. Therefore, the weaker SST produce a weaker zonal mean warming in the tropical troposphere and in the tropical lowermost stratosphere. Second, the largest zonal mean response is observed in the extratropics in both types of ENSO but in different hemispheres: the SH during El Niño Modoki events and the NH during canonical El Niño events.

[24] As explained in section 1, the canonical El Niño signal reaches the NH extratropical stratosphere via ultra-long Rossby waves that propagate upward from the troposphere and dissipate in the stratosphere. Then, wave dissipation decelerates the zonal mean zonal wind and, as a consequence, the Brewer–Dobson circulation intensifies from the tropics to the NH Pole, and an anomalous adiabatic warming appears in the polar region [*García-Herrera et al.*, 2006].

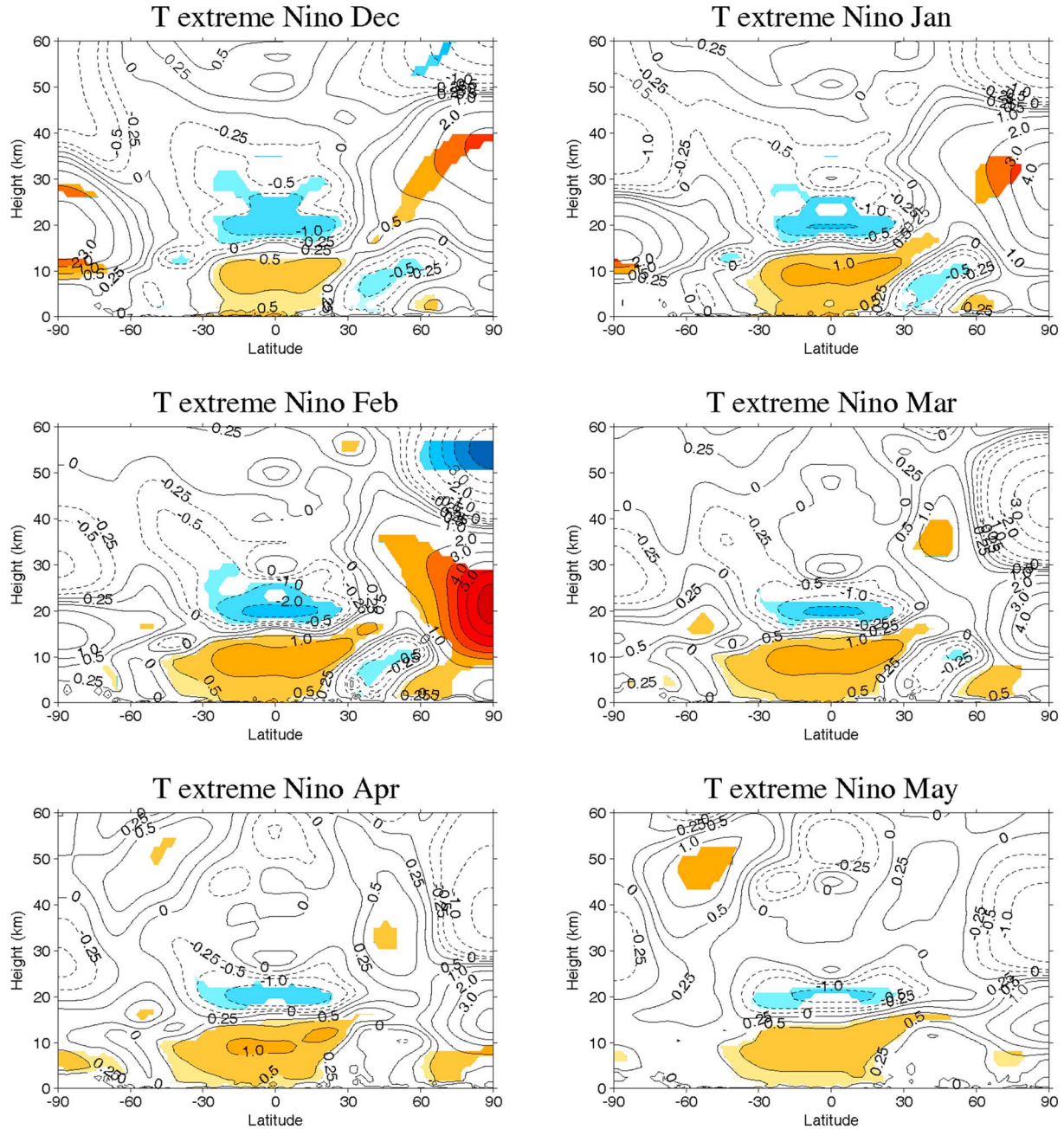


Figure 6. Cross section (height vs. latitude) of the composites of zonal mean temperature anomalies for canonical El Niño extreme events from December to May as explained in the text. Colored regions are significant at the 95% level according to a Monte Carlo test. Contours are drawn every 0.25 K from 0 to ± 0.5 K, every 0.5 K from ± 0.5 to ± 1.0 K and every 1.0 K from ± 1.0 to ± 6.0 K.

[25] To understand the differences between El Niño Modoki and canonical El Niño signals at polar latitudes, Rossby wave propagation and dissipation are analyzed by means of the Eliassen-Palm flux (EP flux) and its divergence [Edmon *et al.*, 1980]. Figure 7 shows El Niño Modoki composites of EP flux for December and January, when the largest significant signal is present. During these months, anomalous upward propagation occurs at midlatitudes in both hemispheres. In the NH, wave propagation intensifies

up to the stratopause in January, while in the SH, the propagation intensifies mainly up to 30 km height. This is related to the background zonal mean zonal winds. Upward Rossby wave propagation is favored by westerly winds, which are present in the entire stratosphere in the NH during boreal winter months. The wave forcing on the background mean flow is illustrated by the divergence of the EP flux (colored areas in Figure 7 indicate significant anomalies). In the SH midlatitudes, anomalous negative EP flux divergence

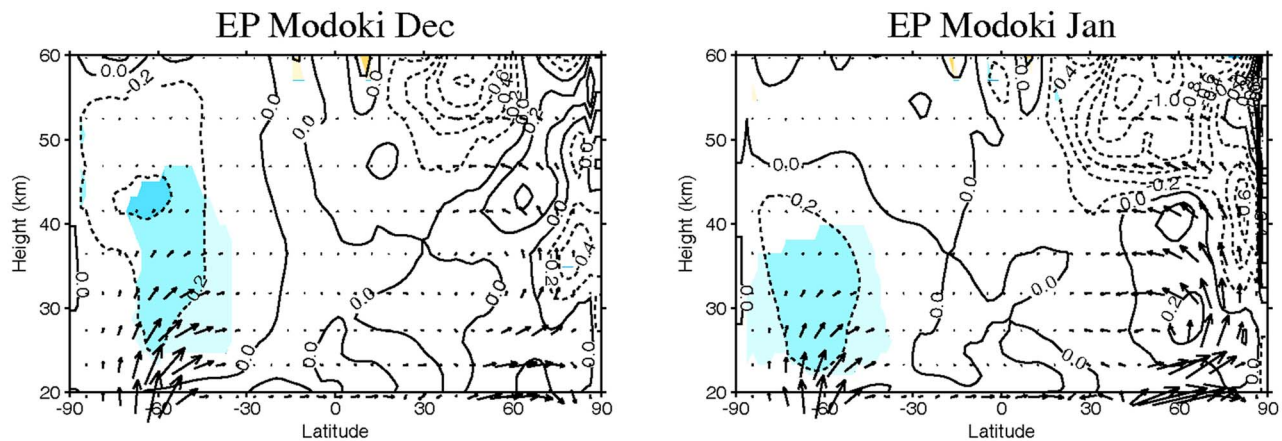


Figure 7. Cross section (height vs. latitude) of the composites of Eliassen-Palm (EP) flux (arrows) and the divergence of the EP flux (contoured) for El Niño Modoki events in December and January, as explained in the text. Colored regions are significant at the 95% level according to a Monte Carlo test. Contours are drawn every $0.2 \text{ m s}^{-1} \text{ day}^{-1}$.

is observed in December and January, which indicates anomalous wave dissipation. This anomalous dissipation in December and January is consistent with the simultaneous anomalous propagation, the consequent deceleration of the mean flow and the anomalous warming shown in Figure 5. In the NH high latitudes, upward wave propagation occurs but the wave forcing is not significant. Thus, no significant impact on the mean flow and temperature is simulated, as can be seen in Figure 4.

[26] In short, when Rossby waves dissipate in the stratosphere, mainly in the SH during El Niño Modoki events and in the NH during canonical El Niño, they decelerate the zonal wind, the stratospheric mean meridional circulation intensifies, and an anomalous downwelling occurs in the polar regions, increasing the temperature there. Hence, the same mechanism by which the signal propagates into the stratosphere in the extratropics operates for El Niño Modoki and canonical El Niño, despite the fact that significant effects take place in different hemispheres in the two cases.

4. Tropospheric Forcing

[27] In the previous section, differences between El Niño Modoki and canonical El Niño stratospheric signals have been identified in the polar region and related to hemispheric differences in wave forcing. Next, we will show that these differences are related to changes in tropospheric ENSO teleconnection patterns and tropical convection between the two types of events.

[28] The main teleconnections associated with ENSO are observed in the Pacific Ocean: the PNA, whose relation to ENSO was explained by *Hoskins and Karoly* [1981]; and the Pacific South American (PSA) pattern, described, among others, by *Mo and Higgins* [1998]. In the NH, the PNA has four centers of action: a high center located in the Pacific Ocean, south of Hawaii; an Aleutian Low that deepens over the North Pacific; a high pressure that develops over the western part of North America; and a low pressure over the southeastern United States. *Weng et al.* [2009] suggested

that the described PNA pattern typical of a warm ENSO events might be a mixture of two different wave trains related to canonical El Niño and El Niño Modoki. This suggests that the PNA teleconnection pattern should be studied separately for the two phenomena. To do so, composites of eddy geopotential height anomalies, computed as the total field minus the zonal mean, have been analyzed for El Niño Modoki and canonical El Niño events at 500 hPa from December to March (Figure 8).

[29] In the NH, a wave train resembling the PNA pattern is simulated during both Modoki and ENSO events in the middle troposphere (500 hPa). During El Niño Modoki events, the full PNA pattern is not clearly observed until February, and the negative anomalies over the Aleutian Low are very weak in December and January. However, during canonical El Niño events, a very clear PNA pattern appears already in December (Figure 8e), coinciding with the largest significant anomalies in upward propagation and dissipation of Rossby waves (not shown). The pattern is present throughout the winter season and disappears in March–April, as described by *Barnston and Livezey* [1987]. According to studies by *Garfinkel and Hartmann* [2008], *Garfinkel et al.* [2010] and *Hegyi and Deng* [2011], this deepening of the Aleutian Low plays a key role in enhancing the climatological wave number-1 component of the planetary wave and the subsequent upward propagation into the stratosphere. Hence, the intensity and duration of the PNA pattern in early winter modifies the upward propagation and varies depending on the type of event. In addition, the location of the centers of action also differs with respect to the pattern described by *Horel and Wallace* [1981]. The centers (especially the positive anomaly located in North America) are displaced westward during El Niño Modoki events and located farther eastward during canonical El Niño events. This modulation of the PNA pattern is consistent with the position of the SST anomalies in the tropical Pacific Ocean typical of each event as explained earlier.

[30] In the SH, a PSA wave train is simulated in both types of El Niño event (Figure 8). During El Niño Modoki, the

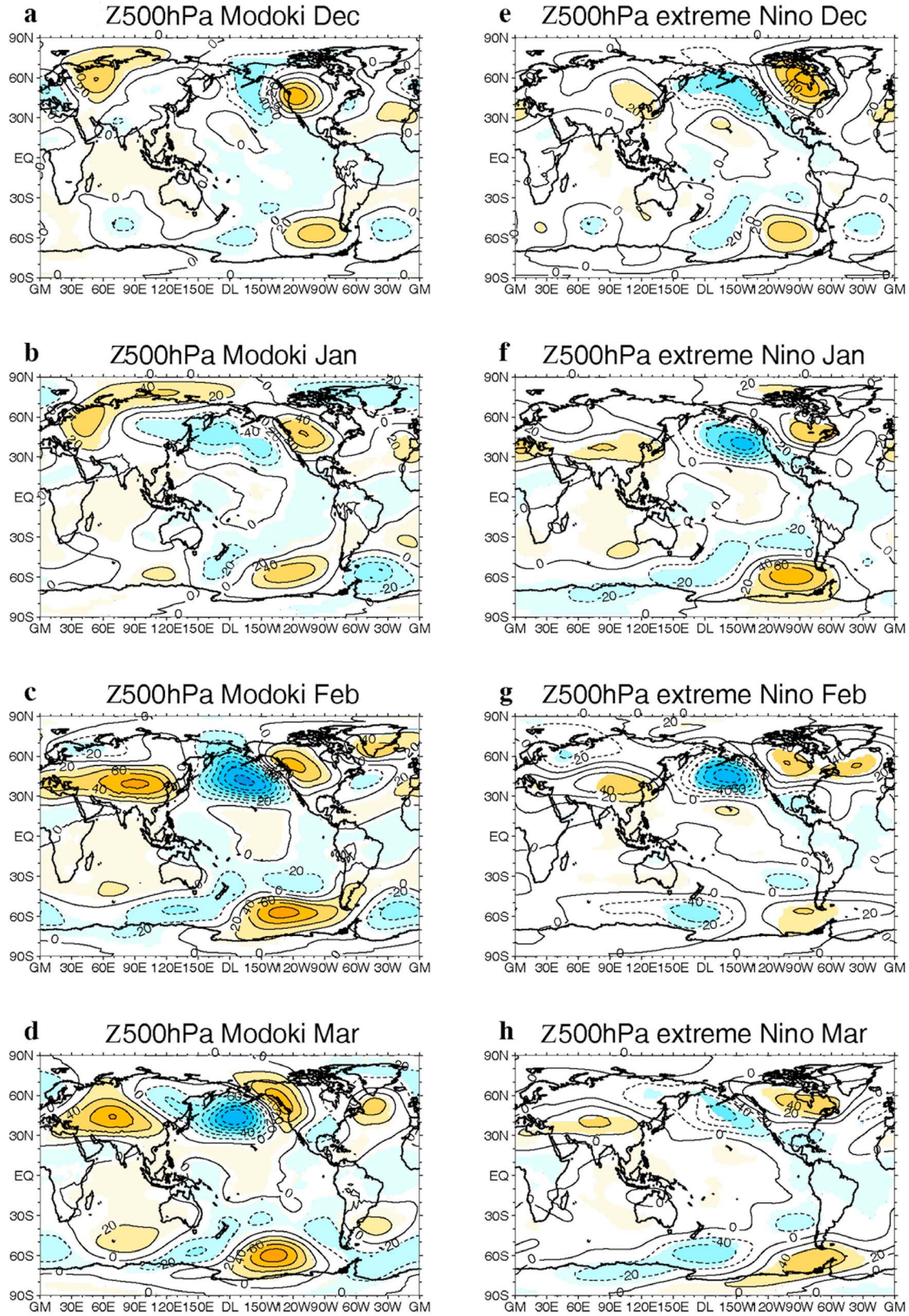


Figure 8. Composites of eddy geopotential height anomalies at 500 hPa for (a–d) El Niño Modoki and (e–h) canonical El Niño extreme events from December to March as explained in the text. Colored regions are significant at the 95% level according to a Monte Carlo test. Contours are drawn every 20 m.

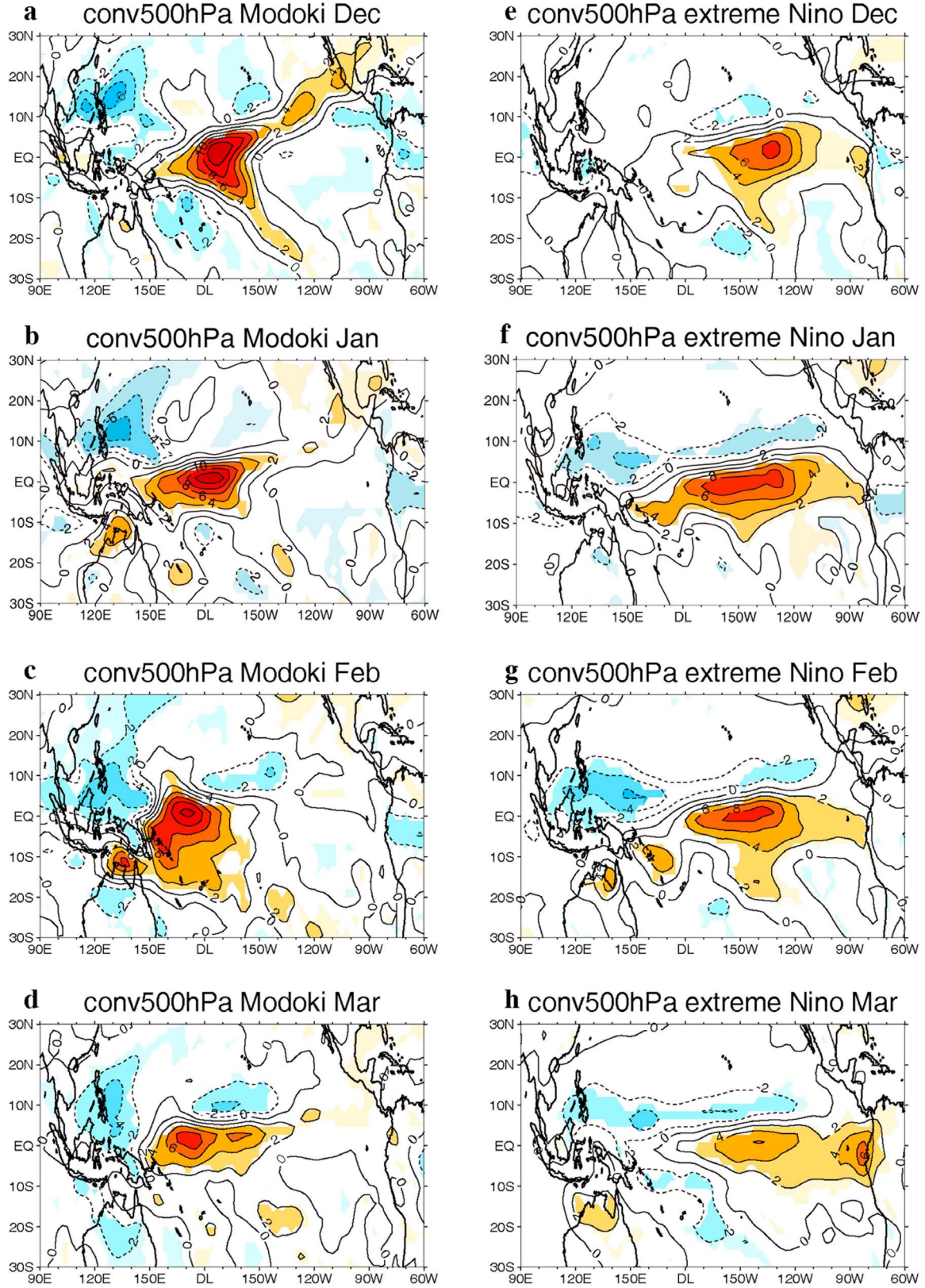


Figure 9. Composites of convection anomalies for (a–d) El Niño Modoki and (e–h) canonical El Niño extreme events from December to March as explained in the text. Colored regions are significant at the 95% level according to a Monte Carlo test. Contours are drawn every 2 K s⁻¹.

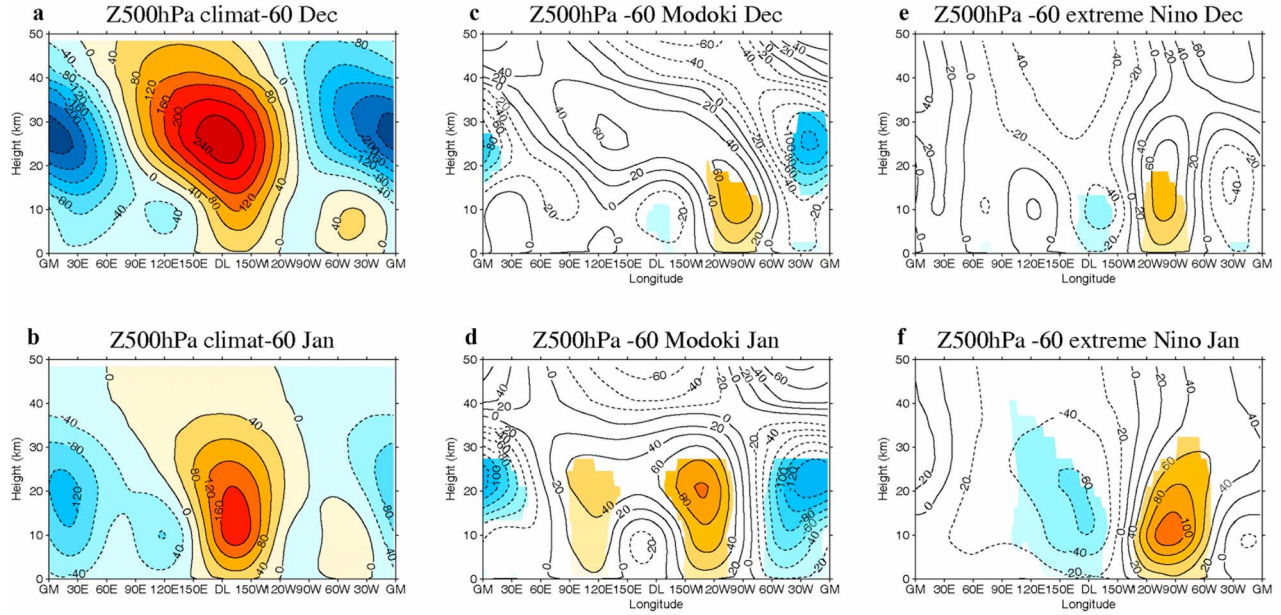


Figure 10. (a–b) Geopotential height eddy climatology and (c–f) composites of eddy geopotential height anomalies for El Niño Modoki (Figures 10c and 10d) and canonical El Niño (Figures 10e and 10f) at 60°S in December and January, as explained in the text. Colored regions are significant at the 95% level according to a Monte Carlo test. Contours are drawn every 40 m in Figures 10a and 10b and every 20 m in Figures 10c–10f.

PSA wave train comprises five centers of action extending from the anticyclone in the subtropics over the dateline, poleward over the south Pacific to South America. There is a low over New Zealand; a high in the central south Pacific, close to the Antarctica; a low over the central tropical Pacific; a high over the Patagonia; and a low to the west of the Islas Malvinas. This pattern reaches maximum intensity in February and decays as boreal winter ends, disappearing in April (not shown). During canonical El Niño events (Figures 8e–8h), a weak PSA (with fewer centers of action) is simulated mainly in January. Therefore, despite weaker SSTA in El Niño Modoki events compared to canonical El Niño, a stronger and more coherent PSA pattern is simulated in the SH. This could contrast with the results of *Mo and Higgins* [1998], who found a strong and coherent PSA pattern during ENSO events. However, their results likely include both canonical and Modoki events as *Weng et al.* [2009] indicated in the case of the PNA pattern discussed above.

[31] Previous studies have related changes in SH circulations to tropical convection. *Karoly* [1989] identified tropical convection as the triggering factor of the PSA in response to ENSO. *Mo and Higgins* [1998] analyzed outgoing longwave radiation (OLR) composites and showed that the PSA modes were associated with changes in convection in the tropical Pacific Ocean. In particular, for El Niño Modoki and canonical El Niño, *Weng et al.* [2009] found that the differences in intensity and location of convection between the two types of events were related to changes in climatic patterns outside the tropics. We have analyzed the evolution of the tropical convection during one year around the peak of the ENSO event, starting in August;

however, only those months with the largest convective anomalies are shown. Composites of convective heating rates at 500 hPa for El Niño Modoki are shown in Figures 9a–9d and for canonical El Niño in Figures 9e–9h. Convection intensifies in both cases in the central tropical Pacific, although the anomalies are higher during El Niño Modoki (12 K s^{-1}) than canonical El Niño (8 K s^{-1}). Their location in longitude is also very different: convection anomalies are located around the dateline and extend westward (up to about 150°E) for El Niño Modoki, while for canonical El Niño events they spread east of the dateline toward the easternmost part of the Pacific Ocean.

[32] As noted earlier, these differences in the location of the anomalous heating rates are consistent with differences in SSTA between the two types of events. In fact, *Kug et al.* [2009] stated that SSTA in the central-western Pacific are much more effective at inducing anomalous convection compared with the eastern Pacific because of the warmer background SST in the former region. They also stated that this makes the global impacts of El Niño Modoki comparable with canonical El Niño, despite its relatively small SSTA (see our Figure 3). To investigate why the different positions of anomalous convection result in stronger upward propagation of Rossby waves in the SH, Figure 10 shows vertical cross sections at 60°S of the climatological eddy geopotential height field (Figures 10a and 10b) and eddy anomalies (Figures 10c–10f) composited for El Niño Modoki and canonical El Niño events for December and January. The comparison of the eddy anomalies with the eddy climatological field reveals that the anomalies interfere more constructively with the climatology during El Niño Modoki events; while, for the canonical El Niño (Figures 9e and 9f),

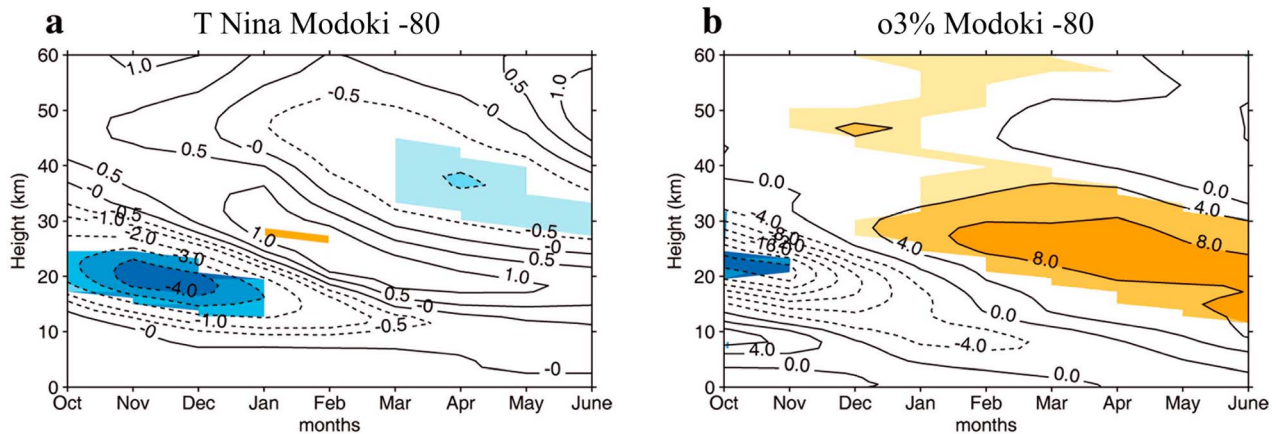


Figure 11. October–June composites of (a) zonal mean temperature anomalies at 80°S for La Niña Modoki events using WACCM3.5 and (b) the percentage change in ozone anomalies at 80°S for El Niño Modoki events. Colored regions are significant at the 95% level according to a Monte Carlo test. Contours are drawn every 0.5 K from 0 to ± 1.0 K and every 1.0 K from ± 1.0 to ± 5.0 K in Figure 11a and 4% in Figure 11b.

the eastward displacement of the anomalies leads to more destructive interference between the anomalous field and the climatology (in particular around the dateline).

5. Discussion

[33] It is clear now that ENSO Modoki has a significant impact on the SH polar stratosphere. A significant warming is present in this region during El Niño Modoki events, related to an enhancement of the PSA teleconnection pattern, which in turn, is intensified by the larger intensity and westward location of convective anomalies compared with canonical ENSO. In fact, we have shown that the longitudinal position plays a key role in the intensification of the PSA teleconnection pattern and, hence, in the differences in extratropical stratospheric signals.

[34] The cold phase of ENSO Modoki, La Niña Modoki, also affects the stratosphere in the SH. In this case, a significant anomalous cooling over the lower SH polar stratosphere appears in October, propagates downward with time, and disappears in January. Figure 11a shows the zonal mean temperature anomalies at 80°S for the cold Modoki events, similar to Figure 5a for warm Modoki events. Compared to the warm phase, the temperature signal of the cold Modoki phase starts a few months earlier in the SH polar stratosphere and reaches its largest intensity at lower stratospheric heights. The opposite signal in temperature in the SH polar stratosphere is related to negative anomalies in convection westward of the dateline and an opposite PSA pattern than that present during warm Modoki events.

[35] El Niño Modoki not only affects extratropical stratospheric zonal mean temperatures and winds but also chemical species such as ozone. The temporal evolution of ozone at 80°S composited for El Niño Modoki events is shown in Figure 11b. A significant increase in ozone (up to 8%) compared to its climatological values is simulated in the lower stratosphere from February to June and it follows the zonal mean temperature anomalies (Figure 5a). This is as expected, because of the anomalous downwelling present at

polar latitudes in response to anomalous wave dissipation and it is also consistent with the adiabatic warming. This increase is of similar magnitude (in percentage) to that obtained in the lowermost tropical stratosphere during warm ENSO events [Randel *et al.*, 2009; Calvo *et al.*, 2010]. On the other hand, the percentage increase in ozone obtained in the SH for El Niño Modoki events almost doubles the ozone anomalies generated in the NH during canonical El Niño events (not shown).

[36] Overall, WACCM3.5 shows a coherent El Niño Modoki impact in the SH stratosphere in zonal mean zonal winds, temperature, and ozone. Similar signals in temperature have been found in temperature in the lowermost Antarctic stratosphere when studying the response of this region to warm pool ENSO events in different reanalysis data sets (NCEP, ERA-40 and MERRA) [Hurwitz *et al.*, 2011b] and also in time-sliced simulations performed with GEOS V2 CCM [Hurwitz *et al.*, 2011a]. They found significant anomalous warming during warm N4 events in the polar stratosphere in ERA-40 reanalysis data in austral spring (November–December) associated with a southward displacement of the SPCZ. Despite obtaining a similar response in the SH polar stratosphere, we have shown that, in WACCM3.5, this may be attributed to an intensification and westward displacement of the convection anomalies. On the other hand, in Hurwitz *et al.*'s [2011b] study, MERRA and NCEP–National Center for Atmospheric Research (NCAR) reanalysis data sets showed significant N4 signal only during the easterly phase of the QBO. Owing to the short observational record, the number of cases in each composite in one single realization was small, especially when stratifying with respect to the QBO phase. Therefore, the conclusions of Hurwitz *et al.* were somewhat limited, as the authors themselves recognized. In a follow-up study using GEOS V2 CCM [Hurwitz *et al.*, 2011a], the role of the QBO was difficult to assess because of the lack of enough penetration of the QBO signature in the lower stratosphere–upper troposphere, although the model did reproduce the observed signals over the SH polar cap. The fact that both time-sliced

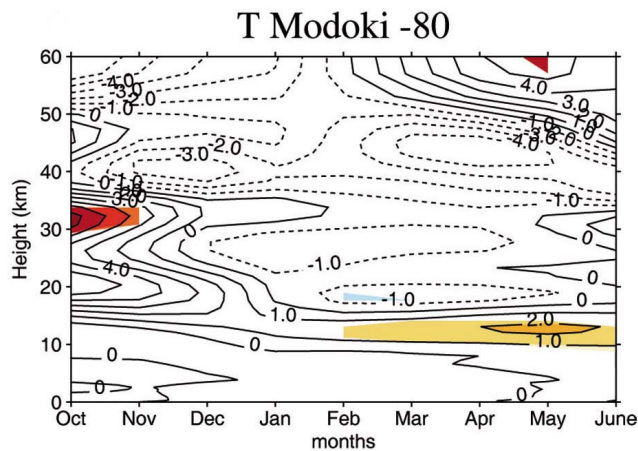


Figure 12. October–June composites of zonal mean temperature anomalies at 80°S for El Niño Modoki events using ERA-40. Colored regions are significant at the 95% level according to a Monte Carlo test. Contours are drawn every 1.0 K.

simulations (used by *Hurwitz et al.* [2011a]) and transient runs (employed in the present study) of two different CCMs are able to simulate anomalous polar stratospheric warming in the SH during warm pool events indicates that this is a robust signal, despite differences in timing and amplitude.

[37] In addition, the impact of El Niño Modoki impact on the stratosphere has also been reproduced in a previous version of WACCM (WACCM1b) [see *Sassi et al.*, 2004]. The WACCM1b simulation used by *Sassi et al.* [2004] had no interactive chemistry, did not simulate or impose a QBO and was run under solar minimum conditions; therefore, variability associated with the 11 year solar cycle was excluded. In this sense, this was a cleaner experiment wherein to analyze the impact of El Niño Modoki events in the stratosphere without the additional complications from other sources of variability. Despite these differences, both versions of the model show a significant warming in the SH polar stratosphere. In the case of WACCM3.5, most of El Niño Modoki events coincide with the easterly phase of the QBO, as *Hurwitz et al.* [2011a, 2011b] pointed out in the case of the reanalysis data sets. Note that the QBO in WACCM3.5 is relaxed to observed tropical winds [Matthes et al., 2004]. However, in WACCM1b, weak easterlies are simulated in the entire tropical stratosphere without westerlies above or below, and therefore, no QBO structure is present. In this sense, our results suggest that the effect of El Niño Modoki events in the stratosphere does not depend on the phase of the QBO, at least in WACCM simulations. This is in agreement with the results obtained by *Hurwitz et al.* [2011a], who used GEOS V2 CCM to simulate the response of the Antarctic polar stratosphere to N4 events and found the Antarctic response insensitive to the phase of the QBO.

[38] Finally, to compare directly the anomalous warming of the SH stratosphere in WACCM3.5 and ERA-40 data, Figure 12 shows the temporal evolution of zonal mean temperature for El Niño Modoki composites in ERA-40, analogous to Figure 5a for WACCM3.5. A multiple linear regression analysis, similar to that applied to WACCM3.5 simulations, has been applied to ERA-40 data. Significant

positive anomalies up to 5.5 K are present at high latitudes between 30 and 35 km in October during El Niño Modoki events. In later months, the warming appears at lower altitudes and becomes significant again from February to June. The agreement between the model and reanalysis is fairly good, although the anomalous warming is stronger and appears earlier in ERA-40 data, as shown by *Hurwitz et al.* [2011b] (their Figure 6a; November–December averages). The weaker anomalies in WACCM3.5 might be caused by the four ensemble members used in WACCM3.5 versus the one single realization of the real world in ERA-40. Note that GEOS V2 CCM also simulated weaker anomalies in this region compared to reanalysis data sets. The differences in timing are probably related to the overestimation of westerly winds in WACCM3.5 in the SH stratosphere: stronger westerly winds reach higher altitudes in the model than in observations during boreal winter months and the polar vortex breaks down too late in spring compared to observations [Butchart et al., 2010], which can explain why the simulated signal lasts longer than the observed one. Overall, despite a few differences between ERA-40 and WACCM, both reanalysis and model show significant anomalous warming in the SH polar stratosphere during El Niño Modoki that is not present during canonical El Niño.

6. Conclusions

[39] In the last decades, a variant of the El Niño phenomenon, referred to as WP El Niño, CP El Niño, or El Niño Modoki, has become more frequent [Yeh et al., 2009 or Ashok et al., 2007]. This type of El Niño event differs from the canonical El Niño in frequency, amplitude, and location of the warm SST, which are located in the central Pacific at or west of the dateline. Differences in teleconnection patterns between these two types of ENSO have also been reported [Weng et al., 2007, 2009]. Here we characterized the signal of ENSO Modoki in the stratosphere in comparison to that from canonical ENSO by using four different realizations of NCAR’s state-of-the-art CCM WACCM3.5, over the 1979–2004 period. The main findings are summarized next:

[40] 1. A significant anomalous warming in the SH polar stratosphere occurs during El Niño Modoki events, not observed during canonical ENSO episodes. This anomalous warming is accompanied by a significantly weaker SH polar vortex and a significant increase in ozone anomalies. We have shown that, in WACCM3.5, these effects are the result of a strong El Niño Modoki PSA tropospheric teleconnection pattern in the SH related to an enhancement of the tropical convection west of the dateline. The intensified PSA during El Niño Modoki events favors anomalous upward propagation of Rossby waves to the lower stratosphere, where they dissipate and generate anomalous downwelling over the polar cap and, therefore, a significantly warmer polar stratosphere and weaker polar vortex during boreal winter months.

[41] 2. El Niño Modoki events have no significant impact in the NH polar stratosphere. This is in contrast with Canonical ENSO events, which have their largest stratospheric signals in this region. Although the PNA strengthens in the troposphere during El Niño Modoki, the Aleutian Low is weaker than the one seen in canonical El Niño, which is a

relevant factor in the upward propagation of the waves into the stratosphere. Besides, its anomalous centers are located westward, compared to extreme N3 events, following the SSTA structure.

[42] 3. In the tropics, the anomalous warming of the tropical troposphere and cooling of the lower stratosphere present during canonical El Niño events weakens during El Niño Modoki episodes, and it is not so persistent. This is directly related to the weaker SSTA generated by El Niño Modoki events compared to canonical El Niño.

[43] 4. The cold phase of ENSO Modoki, La Niña Modoki, produces a significant anomalous cooling in the lower SH polar stratosphere from October to February.

[44] The good agreement among different versions of the model and between the model and reanalysis data, despite differences in amplitude and timing, indicate that El Niño Modoki signal in the SH polar stratosphere is real and consistent. Still, several questions remain open: additional simulations would be necessary to determine the possible role of the QBO on the SH polar signal during El Niño Modoki events. A more detailed analysis is needed to fully understand how changes in the location of convection and SSTA affect tropospheric teleconnections in both hemispheres. This last question will be addressed in future research. Brönnimann *et al.* [2004] and Cagnazzo and Manzini [2009], among others, showed how canonical El Niño events could influence tropospheric weather patterns in Europe. Thompson *et al.* [2005] also linked tropospheric and stratospheric anomalies through changes in the polar vortex. Whether or not the stratospheric signature of El Niño Modoki events can propagate back to the troposphere and affect tropospheric climate, as suggested by the zonal mean zonal winds shown in Figure 5b, is definitely interesting to investigate. Finally, it is important to highlight that if these events are becoming more frequent, as has previously been suggested by Yeh *et al.* [2009] and Ashok *et al.* [2007], their stratospheric effects will need to be considered when analyzing future climate predictions.

[45] **Acknowledgments.** The authors are very thankful to Rolando R. Garcia for multiple fruitful discussions of some parts of the manuscript. D. E. Kinnison is also acknowledged for providing the WACCM3.5 simulations used in this study. I. Zubiaurre was supported by the Spanish Ministry of Education and Sciences under TRODIM project. N. Calvo has been supported by the advanced study program from the National Center for Atmospheric Research (ASP-NCAR).

References

- Ashok, K., and T. Yamagata (2009), Climate change: The El Niño with a difference, *Nature*, **461**, 481–484, doi:10.1038/461481a.
- Ashok, K., S. Behera, A. S. Rao, H. Y. Weng, and T. Yamagata (2007), El Niño Modoki and its teleconnection, *J. Geophys. Res.*, **112**, C11007, doi:10.1029/2006JC003798.
- Barnston, A. G., and R. E. Livezey (1987), Classification, seasonality and persistence of low-frequency atmospheric circulation patterns, *Mon. Weather Rev.*, **115**, 1083–1126, doi:10.1175/1520-0493(1987)115<1083:CSAPOL>2.0.CO;2.
- Bell, C. J., L. J. Gray, A. J. Charlton-Perez, M. M. Joshi, and A. A. Scaife (2009), Stratospheric communication of El Niño teleconnections to European winter, *J. Clim.*, **22**, 4083–4096, doi:10.1175/2009JCLI2717.1.
- Brönnimann, S., J. Luterbacher, J. Staehelin, T. M. Svendby, G. Hansen, and T. Svenoe (2004), Extreme climate of the global troposphere and stratosphere in 1940–1942 related to El Niño, *Nature*, **431**, 971–974, doi:10.1038/nature02982.
- Butchart, N., *et al.* (2010), Stratospheric dynamics, in *Report on the Evaluation of Chemistry-Climate Models*, SPARC Rep. 5, edited by V. Eyring, T. G. Shepherd, and D. W. Waugh, pp. 109–148, Stratos. Processes and Their Role in Clim. Chem. Clim. Models Validation Group, Zurich, Switzerland. [Available at <http://www.sparc-climate.org/publications/sparc-reports/sparc-report-no5/>.]
- Cagnazzo, C., and E. Manzini (2009), Impact of the stratosphere on the winter tropospheric teleconnections between ENSO and the North Atlantic and European region, *J. Clim.*, **22**, 1223–1238, doi:10.1175/2008JCLI2549.1.
- Calvo, N., and D. R. Marsh (2011), The combined effects of ENSO and the 11-year solar cycle on the Northern Hemisphere polar stratosphere, *J. Geophys. Res.*, **116**, D23112, doi:10.1029/2010JD015226.
- Calvo, N., R. R. García, R. García-Herrera, D. Gallego, L. Gimeno, E. Hernández, and P. Ribera (2004), Analysis of the ENSO signal in tropospheric and stratospheric temperatures observed by MSU, 1979–2000, *J. Clim.*, **17**, 3934–3946, doi:10.1175/1520-0442(2004)017<3934:AOTESI>2.0.CO;2.
- Calvo, N., M. A. Giorgetta, R. García-Herrera, and E. Manzini (2009), Nonlinearity of the combined warm ENSO and QBO effects on the Northern Hemisphere polar vortex in MAECHAM4 simulations, *J. Geophys. Res.*, **114**, D13109, doi:10.1029/2008JD011445.
- Calvo, N., R. R. García, W. J. Randel, and D. R. Marsh (2010), Dynamical mechanism for the increase in tropical upwelling in the lowermost tropical stratosphere during warm ENSO events, *J. Atmos. Sci.*, **67**, 2331–2340, doi:10.1175/2010JAS3433.1.
- Edmon, H. J., Jr., B. J. Hoskins, and M. E. McIntyre (1980), Eliassen-Palm cross sections for the troposphere, *J. Atmos. Sci.*, **37**, 2600–2616, doi:10.1175/1520-0469(1980)037<2600:EPCSFT>2.0.CO;2.
- Free, M., and D. J. Seidel (2009), Observed El Niño–Southern Oscillation temperature signal in the stratosphere, *J. Geophys. Res.*, **114**, D23108, doi:10.1029/2009JD012420.
- García-Herrera, R., N. Calvo, R. R. García, and M. A. Giorgetta (2006), Propagation of ENSO temperature signals into the middle atmosphere: A comparison of two general circulation models and ERA-40 reanalysis data, *J. Geophys. Res.*, **111**, D06101, doi:10.1029/2005JD006061.
- García, R. R., D. R. Marsh, D. E. Kinnison, B. A. Boville, and F. Sassi (2007), Simulations of secular trends in the middle atmosphere, 1950–2003, *J. Geophys. Res.*, **112**, D09301, doi:10.1029/2006JD007485.
- Garfinkel, C. I., and D. L. Hartmann (2007), Effects of the El-Niño Southern Oscillation and the Quasi-Biennial Oscillation on polar temperatures in the stratosphere, *J. Geophys. Res.*, **112**, D19112, doi:10.1029/2007JD008481.
- Garfinkel, C. I., and D. L. Hartmann (2008), Different ENSO teleconnections and their effects on the stratospheric polar vortex, *J. Geophys. Res.*, **113**, D18114, doi:10.1029/2008JD009920.
- Garfinkel, C. I., D. L. Hartmann, and F. Sassi (2010), Tropospheric precursors of anomalous Northern Hemisphere stratospheric polar vortices, *J. Clim.*, **23**, 3282–3299, doi:10.1175/2010JCLI3010.1.
- Hegyi, B. M., and Y. Deng (2011), A dynamical fingerprint of tropical Pacific Sea surface temperatures on the decadal-scale variability of cool-season Arctic precipitation, *J. Geophys. Res.*, **116**, D20121, doi:10.1029/2011JD016001.
- Horel, J. D., and J. M. Wallace (1981), Planetary-scale atmospheric phenomena associated with the Southern Oscillation, *Mon. Weather Rev.*, **109**, 813–829, doi:10.1175/1520-0493(1981)109<0813:PSAPAW>2.0.CO;2.
- Hoskins, B. J., and D. J. Karoly (1981), The steady linear response of a spherical atmosphere to thermal and orographic forcing, *J. Atmos. Sci.*, **38**, 1179–1196, doi:10.1175/1520-0469(1981)038<1179:TSLROA>2.0.CO;2.
- Hurwitz, M. M., I. S. Song, L. D. Oman, P. A. Newman, A. M. Molod, S. M. Frith, and J. E. Nielsen (2011a), Response of the Antarctic stratosphere to warm pool El Niño events in the GEOS CCM, *Atmos. Chem. Phys.*, **11**, 9659–9669, doi:10.5194/acp-11-9659-2011.
- Hurwitz, M. M., P. A. Newman, L. D. Oman, and A. M. Molod (2011b), Response of the Antarctic stratosphere to two types of El Niño events, *J. Clim.*, **68**, 812–822, doi:10.1175/2011JAS3606.1.
- Ineson, S., and A. A. Scaife (2009), The role of the stratosphere in the European climate response to El Niño, *Nat. Geosci.*, **2**, 32–36, doi:10.1038/ngeo381.
- Kao, H. Y., and J. Y. Yu (2009), Contrasting Eastern-Pacific and Central-Pacific types of El Niño, *J. Clim.*, **22**, 615–632, doi:10.1175/2008JCLI2309.1.
- Karoly, D. J. (1989), Southern Hemisphere circulation features associated with El Niño–Southern Oscillation events, *J. Clim.*, **2**, 1239–1252, doi:10.1175/1520-0442(1989)002<1239:SHCFW>2.0.CO;2.
- Kim, H. M., P. J. Webster, and J. A. Curry (2009), Impact of shifting patterns of Pacific Ocean warming on North Atlantic tropical cyclones, *Science*, **325**, 77–80, doi:10.1126/science.1174062.

- Kug, J. S., F. F. Jin, and S. I. An (2009), Two types of El Niño events: Cold tongue El Niño and warm pool El Niño, *J. Clim.*, **22**, 1499–1515, doi:10.1175/2008JCLI2624.1.
- Manzini E., M. A. Giorgetta, M. Esch, L. Kornbluh, and E. Roeckner (2006), The influence of sea surface temperatures on the Northern winter stratosphere: Ensemble simulations with the MAECHAM5 model, *J. Clim.*, **19**, 3863–3881, doi:10.1175/JCLI3826.1.
- Matthes, K., U. Langematz, L. L. Gray, K. Kodera, and K. Labitzke (2004), Improved 11-year solar signal in the Freie Universität Berlin Climate Middle Atmosphere Model (FUB-CMAM), *J. Geophys. Res.*, **109**, D06101, doi:10.1029/2003JD004012.
- Mo, K. C., and R. W. Higgins (1998), The Pacific–South American modes and Tropical Convection during the Southern Hemisphere winter, *Mon. Weather Rev.*, **126**, 1581–1596, doi:10.1175/1520-0493(1998)126<1581:TPSAMA>2.0.CO;2.
- Randel, W. J., and F. Wu (1996), Isolation of the ozone QBO in SAGE II data by singular-value decomposition, *J. Atmos. Sci.*, **53**, 2546–2559, doi:10.1175/1520-0469(1996)053<2546:IOTOQI>2.0.CO;2.
- Randel, W. J., R. Garcia, N. Calvo, and D. Marsh (2009), ENSO influence on zonal mean temperature and ozone in the tropical lower stratosphere, *Geophys. Res. Lett.*, **36**, L15822, doi:10.1029/2009GL039343.
- Rayner, N. A., D. E. Parker, E. B. Horton, C. K. Folland, L. V. Alexander, D. P. Rowell, E. C. Kent, and A. Kaplan (2003), Global analyses of sea surface temperature, sea ice, and night marine air temperature since the late nineteenth century, *J. Geophys. Res.*, **108**(D14), 4407, doi:10.1029/2002JD002670.
- Sassi, F., D. Kinnison, B. A. Boville, R. R. Garcia, and R. Roble (2004), Effects of El Niño–Southern Oscillation on the dynamical, thermal and chemical structure of the middle atmosphere, *J. Geophys. Res.*, **109**, D17108, doi:10.1029/2003JD004434.
- Stratospheric Processes and Their Role in Climate Chemistry–Climate Models Validation Group (SPARC CCMVal) (2010), Report on the evaluation of Chemistry–Climate Models, *SPARC Rep. 5*, *WCRP-132, WMO/TD-1526*, edited by V. Eyring, T. G. Shepherd, and D. W. Waugh, Zurich, Switzerland. [Available at <http://www.sparc-climate.org/publications/sparc-reports/sparc-report-no5/>.]
- Thompson, D., M. Baldwin, and S. Solomon (2005), Stratosphere–troposphere coupling in the Southern Hemisphere, *J. Clim.*, **62**, 708–715, doi:10.1175/JAS-3321.1.
- Tilmes, S., R. R. Garcia, D. E. Kinnison, A. Gettelman, and P. J. Rasch (2009), Impact of geoengineered aerosols on the troposphere and stratosphere, *J. Geophys. Res.*, **114**, D12305, doi:10.1029/2008JD011420.
- Weng, H., K. Ashok, S. K. Behera, S. A. Rao, and T. Yamagata (2007), Impacts of recent El Niño Modoki on dry/wet conditions in the Pacific rim during boreal summer, *Clim. Dyn.*, **29**, 113–129, doi:10.1007/s00382-007-0234-0.
- Weng, H., K. Behera, and T. Yamagata (2009), Anomalous winter climate conditions in the Pacific rim during recent El Niño Modoki and El Niño events, *Clim. Dyn.*, **32**, 663–674, doi:10.1007/s00382-008-0394-6.
- Yeh, S. H., J. S. Kug, B. Dewitte, M. H. Kwon, B. P. Kirtman, and F. F. Jin (2009), El Niño in a changing climate, *Nature*, **461**, 511–514, doi:10.1038/nature08316.

N. Calvo, Atmospheric Chemistry Division, Advanced Study Program, National Center for Atmospheric Research, PO Box 3000, Boulder, CO 80307, USA.

I. Zubiaurre, Departamento Física de la Tierra, Astrofísica y Astronomía, Universidad Complutense de Madrid, Madrid E-28040, Spain. (izubiaur@fis.ucm.es)